



Highly flexible supercapacitors with manganese oxide nanosheet/carbon cloth electrode

Ying-Chu Chen^a, Yu-Kuei Hsu^b, Yan-Gu Lin^a, Yu-Kai Lin^{c,d}, Ying-Ying Horng^c, Li-Chyong Chen^a, Kuei-Hsien Chen^{a,c,*}

^a Center for Condensed Matter Sciences, National Taiwan University, Taipei 106, Taiwan

^b Department of Opto-Electronic Engineering, National Dong Hwa University, Hualien 97401, Taiwan

^c Institute of Atomic and Molecular Science, Academia Sinica, Taipei 106, Taiwan

^d Department of Physics, National Taiwan University, Taipei 106, Taiwan

ARTICLE INFO

Article history:

Received 28 January 2011

Received in revised form 21 May 2011

Accepted 21 May 2011

Available online 31 May 2011

Keywords:

Supercapacitors

MnO₂

Nanosheet

Flexible

Birnessite

ABSTRACT

We report a simple and cost-effective synthesis of hierarchically porous structure composed of Birnessite-type manganese dioxide (MnO₂) nanosheets on flexible carbon cloth (CC) via anodic electrodeposition technique. Petal-shaped MnO₂, having sheet thickness of a few nm and typical width of 100 nm, with a strong adhesion on CC is observed. This hierarchically porous MnO₂-CC hybrid structure dose exhibit not only excellent capacitance properties, such as up to 425 Fg⁻¹ in specific capacitance, but also high crack resistance owing to its efficient release of bending stress, as observed by cyclic voltammetry and galvanostatic charge/discharge measurements under different curvature of bending configurations. Furthermore, flexible supercapacitors based on this kind of MnO₂ nanosheet/CC electrode showed significantly improved stability in capacitive performance over 3000 cycles under the bending test, which is highly promising for future applications in flexible energy storage device.

© 2011 Elsevier Ltd. All rights reserved.

1. Introduction

With the growing interest in recent years in development of portable and flexible electronics, flexible and safe energy-storage devices based on battery and/or electrochemical capacitors have also attracted increasing attention to power such flexible devices [1–3]. Electrochemical capacitors (also known as supercapacitors) have, especially, shown great potential in recent years to meet the short-term power needs [4–7]. Supercapacitors can be classified into two broad categories, viz. electrical double-layer capacitor and pseudocapacitor, based on their charge-storage mechanism [8–12]. In theory, the capacitive ability of pseudocapacitors, whose electron storage mechanism involves reversible Faradaic reaction, is expected to be higher than that of the double-layer capacitors, wherein the capacitance arises from electrostatic separation at the interface. Transition metal oxides and conducting polymers with several reversible oxidation states/structures are commonly regarded as potential active materials for pseudocapacitors [13–17]. Among them, MnO₂-based supercapacitors have

shown great promise due to their environmental friendly nature, good electrochemical performance in neutral electrolyte, as well as low cost of raw materials [18–20].

It is also well-known that several materials exhibit peculiar and fascinating properties on a nano-scale, superior to their bulk counterparts. Particularly, nanostructural MnO₂ exhibits larger surface area and shorter conduction lengths for electrons and cations; in addition, such structures are amenable to release the bending stress, making it highly attractive for application as electrodes for flexible energy-storage devices. To date, the two main methods used to produce nanosized MnO₂ are hydrothermal approach and electrochemical deposition [21–24]. Under different operating modes, the latter can be easily utilized to deposit a variety of morphologies of MnO₂ on a given substrate without requiring any further process in electrode preparation [15,25]. Moreover, a porous hierarchical nanostructure consisting of nanosized Mn oxides by a simple two-step electrochemical deposition process exhibited high specific capacitance (470 Fg⁻¹) and good cycle stability [26]. In addition, other approaches, such as self-limiting reaction of permanganate with carbon and chemical reaction using permanganate, have also been reported for synthesis of nanosized MnO₂ [27,28]. Typically, two-dimensional and rigid substrates, such as the stainless steel and metal foil, are widely used as current collectors [29,30]. Recently, the potential of composite materials of carbon nanotubes and MnO₂ via layer-by-layer method for flexible supercapacitors have been demonstrated [31,32]. However,

* Corresponding author at: Center for Condensed Matter Sciences, National Taiwan University, Taipei 106, Taiwan. Tel.: +886 2 2366 8232; fax: +886 2 2362 0200.

E-mail addresses: chenlc@ntu.edu.tw (L.-C. Chen), chenkh@pub.iams.sinica.edu.tw (K.-H. Chen).

mechanically flexible carbon fibers woven in form of cloth (carbon cloth, CC), which are commercially available materials as gas diffusion layer in fuel cells [33,34], may be attractive alternative for application as flexible electrodes due to their good electrical conductivity, chemical stability, light weight, flexibility and high porosity. In addition, CC also displays adequate electrochemical properties, making them suitable for electrodeposition of MnO_2 nanostructures. As presented here, our approach does not require any binders or conductive agents; therefore, common problems arising from their residues that lead to reduced electron storage capacity and inconsistent cycle life-time in conventional MnO_2 powder-based supercapacitors can thus be avoided [35].

In the present work, we utilized a simple and cost-effective electroplating approach to directly deposit layered MnO_2 nanostructures on the surface of carbon cloth. The resulting hierarchical electrode with strong adhesion between hybrid petal-shaped MnO_2 and flexible CC not only yields promising capacitive performance due to fast penetration of the electrolyte, but also allows the electrode to be bent without diminution of capacitance, via release of the bending stress through the adjustment of the inter-particle separation.

2. Experimental

2.1. Materials and chemicals

A commercially available CC (E-TEK, USA), with specifications: B-1 Designation A (weave = plain, weight = 116 g m^{-2} , thickness = 0.35 mm , and 0 wt % wet proofing), was used as the supporting material for MnO_2 . Other chemicals used for MnO_2 deposition, viz. H_2SO_4 , $\text{MnSO}_4 \cdot 5\text{H}_2\text{O}$ and Na_2SO_4 , were of analytical-reagent grade from Aldrich.

2.2. Fabrication of MnO_2/CC electrodes

The CC electrode was prepared by bonding a copper wire onto the edge of approximately $1 \times 0.5 \text{ cm}$ rectangle of CC. The bonding of Cu-wire was done by using silver paste, cured for 20 min at 80°C . The bonding pad was covered with epoxide in order to allow exposure of only the CC surface to the electrochemical deposition solutions. MnO_2 was electrochemically deposited onto this electrode in an electrolyte solution of $0.1 \text{ M H}_2\text{SO}_4 + 0.1 \text{ M MnSO}_4 \cdot 5\text{H}_2\text{O}$ under galvanostatic condition of 0.5 mA cm^{-2} for durations of 500, 1000, 1500, 2000, and 2500s, and then rinsed with distilled water. The current density was normalized by the geometric area of CC. The amount of MnO_2 deposited on the CC electrode was determined from the difference in weight of the electrode before and after electrodeposition, using a microbalance with a measurement accuracy of $10 \mu\text{g}$ (Sartorius BP 211D, Germany). The loading level of the active materials was found to be around 0.1–0.6 mg.

2.3. Measurement of the characteristics of MnO_2/CC electrodes

The microstructure and morphology of MnO_2 were investigated by means of field-emission scanning electron microscopy (FESEM, JEOL-6700), X-ray diffraction spectroscopy (Bruker D8 Advance diffractometer), and Raman spectroscopy (Jobin-Yvon LabRAM HR800). The chemical states of the elements were determined by electron spectroscopy (ESCA, Perkin-Elmer model PHI 1600). Electrochemical measurements were conducted using Solartron electrochemical test system (1470E) at ambient temperature. In order to evaluate the electrochemical capacitance performance of MnO_2/CC , cyclic voltammetry (CV) and galvanostatic charge/discharge methods were used. All electrochemical measurements were carried out in $0.1 \text{ M Na}_2\text{SO}_4$ aqueous solution

as electrolyte, using a conventional three-electrode system consisting of the MnO_2/CC electrode as the working electrode, square platinum sheet as the auxiliary electrode, and an Ag/AgCl reference electrode in 3 M KCl solution. All potentials reported in this article are with respect to that of Ag/AgCl (3 M KCl , 0.207 V vs. SHE) reference electrode.

2.4. Assembly of symmetrical MnO_2/CC capacitors

Symmetrical capacitors, $\text{MnO}_2/\text{cellulose}/\text{MnO}_2$ (hereafter referred to MnO_2 capacitor), were assembled with cellulose film as separator by sandwiching the MnO_2/CC electrodes. Cellulose film is the main constituent of paper and an inexpensive insulating separator. Before assembly, the MnO_2/CC electrodes were soaked in an electrolyte of $0.1 \text{ M Na}_2\text{SO}_4$ for about 10 min. This step allowed filling of the pores of polymer matrix by the aqueous electrolyte.

3. Results and discussion

3.1. Morphology

The preparation procedure for MnO_2 nanosheet/CC hybrid electrodes is illustrated schematically in Fig. 1. First, nanostructured MnO_2 was anodically electroplated onto macroporous CC substrates using MnSO_4 as precursor solution. The electrode deposition was carried out in Galvanostatic mode at 0.5 mA cm^{-2} , corresponding to the operational potential of $0.9 \text{ V vs. Ag/AgCl}$ reference electrode, for variable periods of time using $10 \text{ mm} \times 5 \text{ mm}$ CC substrate. Notably, the double layer current in this set-up was only around few tens of μA . The application of higher current further oxidizes the Mn^{2+} precursors into Mn oxidation state of 4. After the electroplating process, nanostructured MnO_2/CC hybrid structure was obtained in hydrated state, which offers an unobstructed electron conduction path. These hierarchical nanocomposite electrodes, which combine macroporous CC as reservoir and MnO_2 nanostructures as active materials, facilitate the access to cations from the electrolyte accompanying the reversible redox between Mn^{3+} and Mn^{4+} oxidation states. Further, the evolution of morphology corresponding to different deposition periods was examined by FESEM, as presented in Fig. 2. The low magnification SEM images, in Fig. 2a, clearly show the uniform distribution of nano-clusters of MnO_2 on carbon fiber surface. With increasing deposition time, the density of nano-clusters gradually increased until the whole carbon fiber surface was fully covered at a deposition time of 2000s. As the deposition time was further increased to 2500s, the nano-clusters of MnO_2 merged together to form a highly fragile contiguous film that easily cleaved due to the curvature of the electrode. However, the other samples with lower deposition times maintained the original MnO_2 nanostructure without apparent damage even after bending the electrodes. Fig. 2b presents the corresponding high magnification SEM images that clearly show each nano-cluster consisting of irregular sheets to form the petal-shaped nanostructure of MnO_2 . These nano-sized MnO_2 clusters exhibit microporous architectures and strong adhesion on CC, giving high active surface area and low interfacial resistance of the electrode. The BET surface areas of the samples were also examined to be $25.5 \text{ m}^2 \text{ g}^{-1}$ for bare CC and $133.2 \text{ m}^2 \text{ g}^{-1}$ for MnO_2/CC composite electrode. The significant increase in the surface area is due to the surface coverage of hierarchical nanoflakes MnO_2 , which is consistent with the observation from the SEM images. With increase in deposition time, the isolated clusters appeared to maintain their petal-shaped structure, while the density of the clusters increased. The optimum uniformity and coverage with petal-shaped MnO_2 nano-cluster was obtained at the deposition time of 2000s. The clusters appeared to consist of irreg-

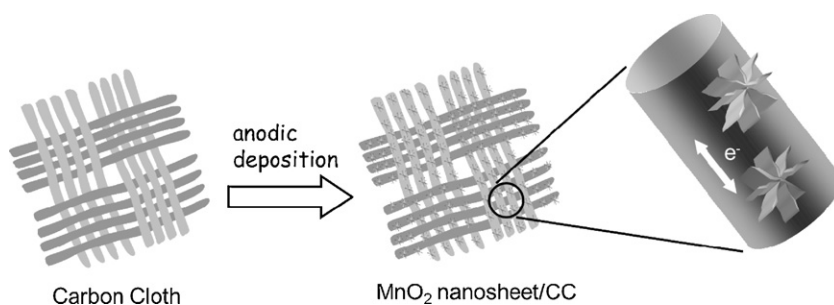


Fig. 1. Schematic diagram for fabrication of MnO_2/CC hybrid electrode.

ular sheets with thickness of a few nm and width of about 100 nm. Such a microstructure ensures optimum utilization of MnO_2 within the diffusion length of the cations. Therefore, this hierarchically porous structure composed of microporous MnO_2 and macroporous CC appears to be a promising candidate for application as electrode of a supercapacitor.

3.2. Structural characterization and composition analysis

Fig. 3a shows the XRD patterns of hybrid MnO_2/CC electrodes prepared at various deposition times. An XRD pattern for CC substrate is also shown for comparison. It can be seen that none of the XRD patterns of the hybrid electrodes with dif-

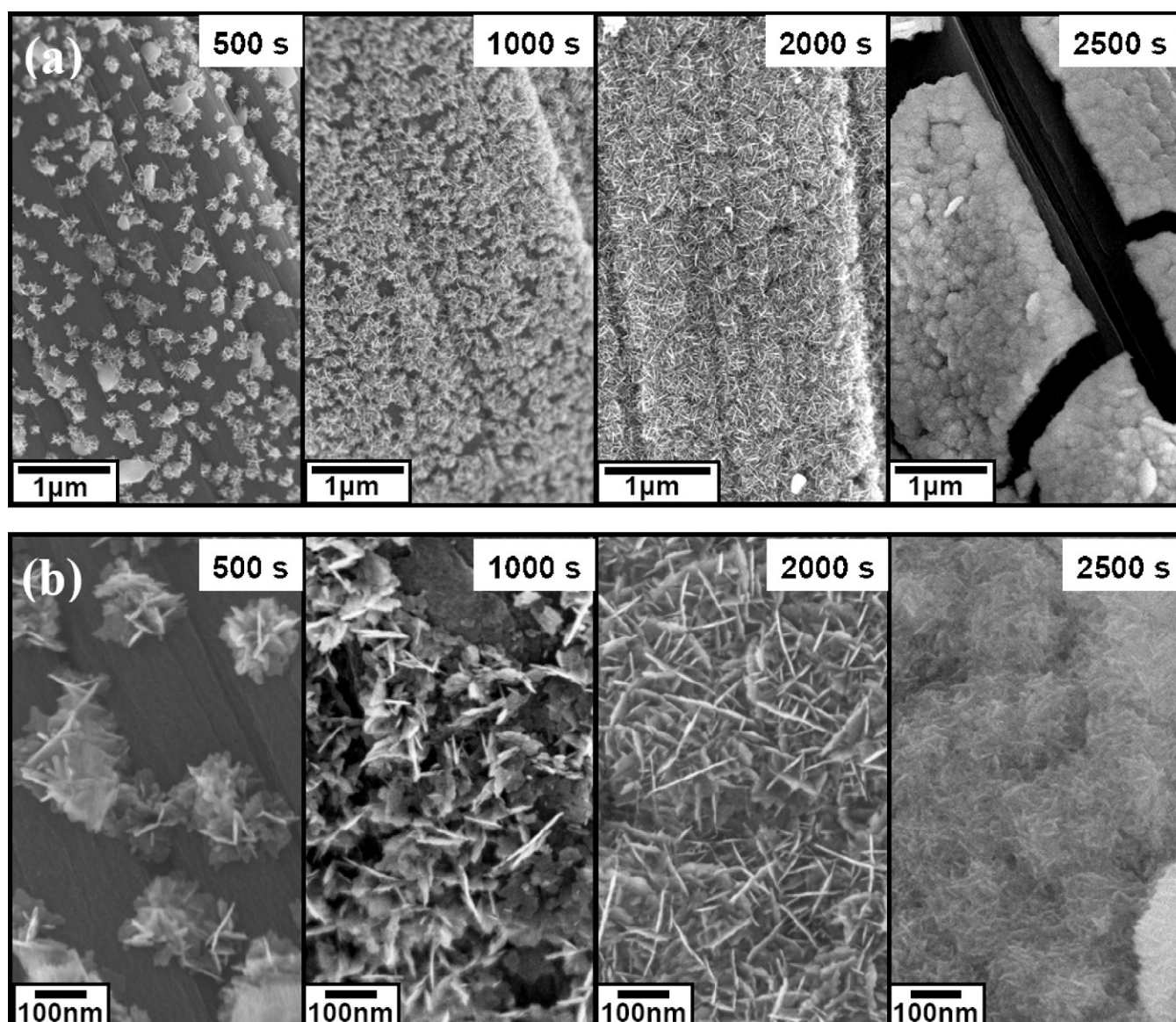


Fig. 2. FESEM micrographs of MnO_2/CC hybrid electrodes, fabricated via anodic electrodeposition, for different deposition times (a) low magnification, (b) high magnification.

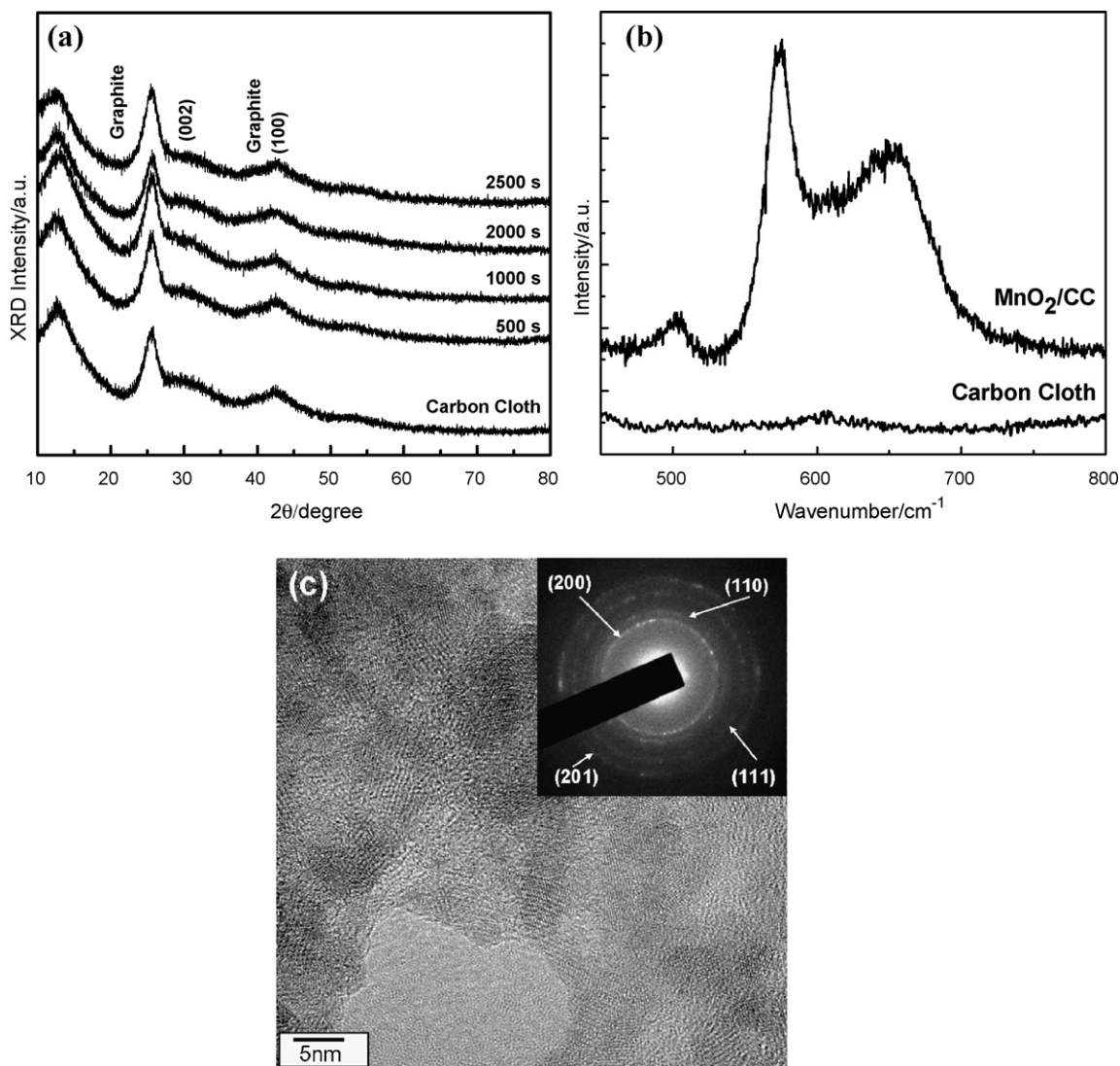


Fig. 3. (a) XRD patterns of MnO_2/CC hybrid electrodes, fabricated via anodic electrodeposition, for different deposition times. (b) Raman spectra of MnO_2/CC hybrid electrodes (deposition time of 2000s) and carbon cloth. (c) TEM image of MnO_2 nanosheets; inset, the corresponding SAED pattern.

ferent deposition periods display any visible diffraction peaks corresponding to MnO_2 ; all of the strong diffraction peaks are associated with graphite. This indicates a long-range disorder of MnO_2 in these composites. However, in order to explore the local structure of MnO_2 nanosheet/CC, Raman microscopy and TEM, which is sensitive to the structural short-range order in amorphous materials, was used. Fig. 3b shows the Raman spectrum of MnO_2 nanosheet/CC hybrid electrode synthesized by anodic electroplating for the deposition time of 2000s. A Raman spectrum of CC is also shown for comparison. Three major features corresponding to MnO_2 can be identified at 500, 575 and 648 cm^{-1} . The strong Raman band at 648 cm^{-1} can be attributed to the symmetric stretching vibration (Mn–O) of the MnO_6 groups [36], while the second strong band located at 575 cm^{-1} is usually attributed to the (Mn–O) stretching vibration in the basal plane of MnO_6 sheet [36]. From these vibrational features, a Birnessite-type MnO_2 with layered structure can be concluded, which also agrees well with the SEM observations. TEM micrographs and corresponding selected area electron diffraction pattern (SAED), shown in Fig. 3c, were taken from the MnO_2/CC electrodes. From TEM image, the layered structure composed of several petal-shaped thin nanosheets. Continuous ring pattern of SAED

also confirmed their nanocrystalline nature. The d-spacings of (200), (110), (111) and (201) measured from the SAED pattern are consistent with Birnessite-type MnO_2 (JCPDS 42-1317) [21].

X-ray photo-electron spectroscopy (XPS) is a most widely used technique for analyzing the chemical states of the surface elements. As shown in Fig. 4a, Mn 2p core level spectrum displays two peaks at binding energies of 654.3 and 642.6 eV corresponding to the spin-orbit doublet attributed to the Mn 2p_{1/2} and Mn 2p_{3/2}. The spin-energy separation of 11.7 eV indicates the formation of MnO_2 [9]. Moreover, the binding energies of Mn 2p_{3/2} electron for Mn^{3+} and Mn^{4+} states are reported to be 641.6 and 642.6 eV, respectively, which further confirms the composition of the deposit as MnO_2 [37]. Fig. 4b shows the O 1s spectrum of the MnO_2 nanosheet/CC electrode, which could be fitted into three main constituent peaks corresponding to different oxygen-containing species, viz. Mn–O–Mn bond at 529.7 eV, Mn–OH bond at 531.8 eV, and H–O–H bond at 534.1 eV [9]. Based on the areas under these peaks, the atomic ratio of Mn to O is estimated to be 1:2.12. Notably, the 534.1 eV XPS peak corresponds to water molecule (H–O–H), which confirms the MnO_2 nanosheet to be in hydrated form.

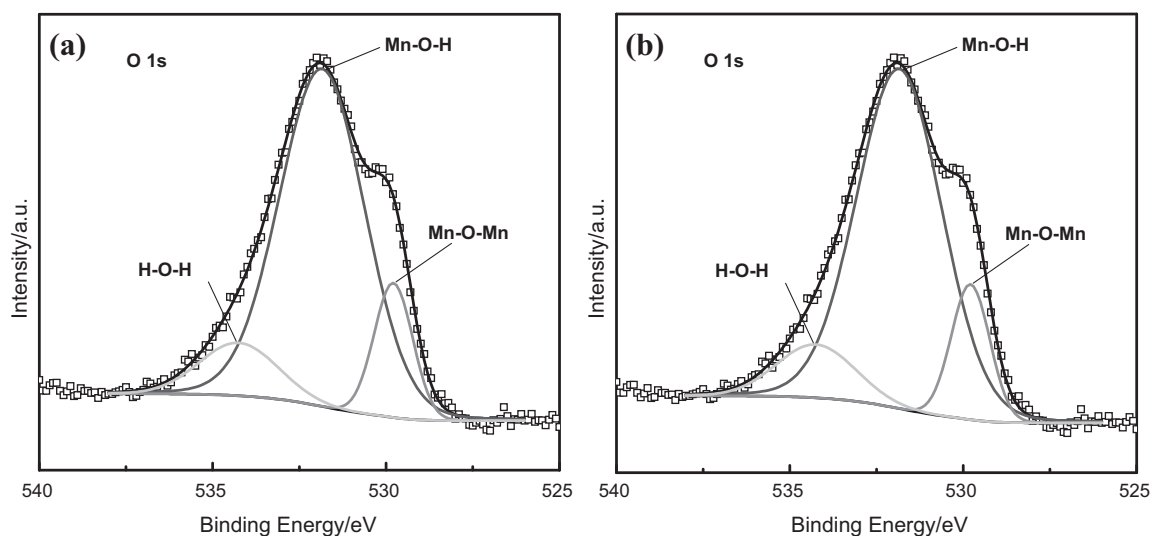


Fig. 4. XPS spectra of (a) Mn 2p core level and (b) O 1s core level for MnO₂/CC hybrid electrodes (deposition time of 2000s).

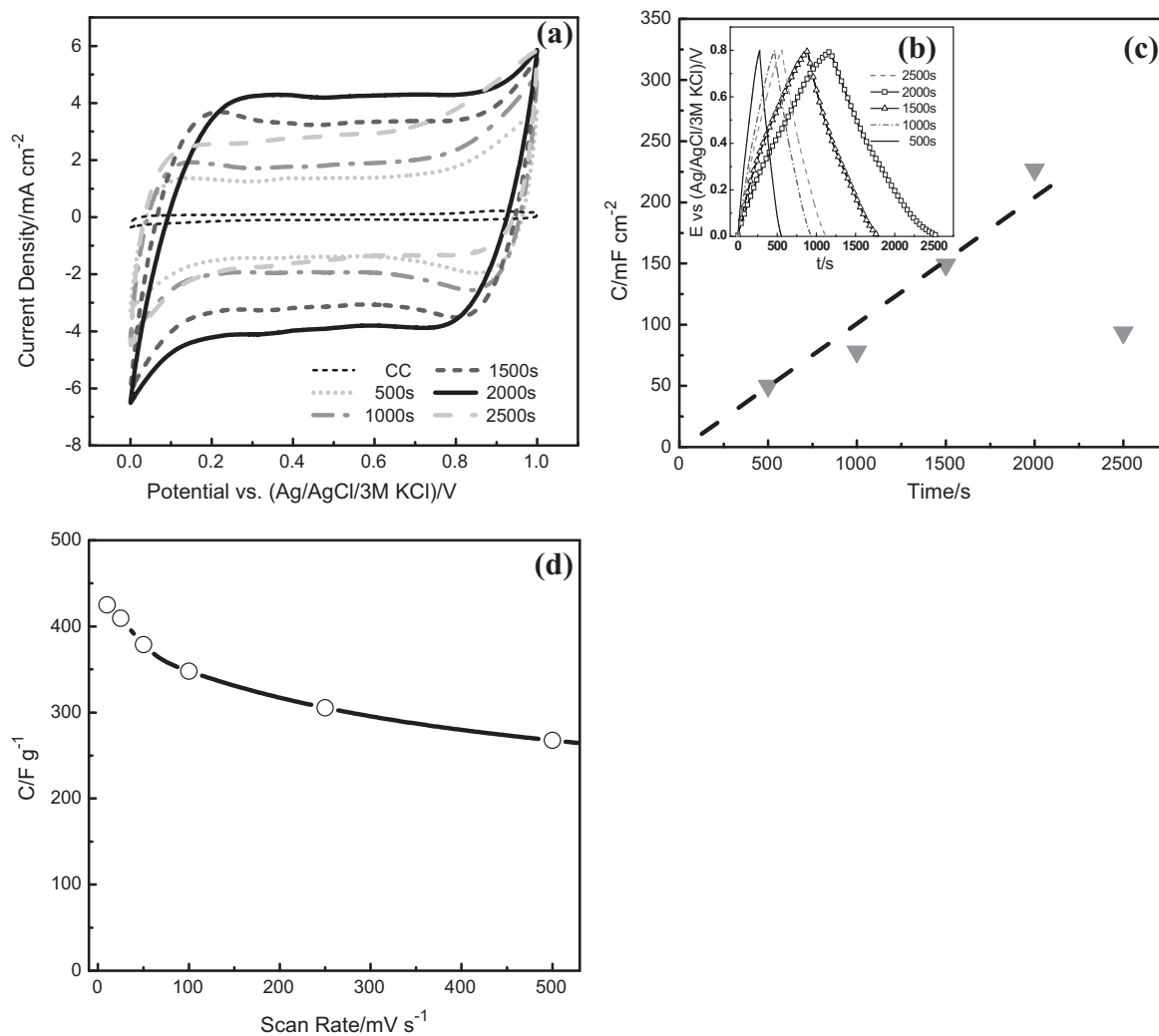


Fig. 5. (a) Cyclic voltammograms of MnO₂/CC hybrid electrodes with different deposition times at a scan rate of 25 mV s⁻¹, (b) charge–discharge curves of MnO₂/CC hybrid electrodes with different deposition times at a fixed current density of 0.13 mA cm⁻², (c) variation in area-normalized capacitance of MnO₂/CC electrodes as a function of deposition time, and (d) dependence of the specific capacitance on the scan rate of CV from 10 mV s⁻¹ to 1000 mV s⁻¹ for MnO₂/CC hybrid electrodes (deposition time of 2000s).

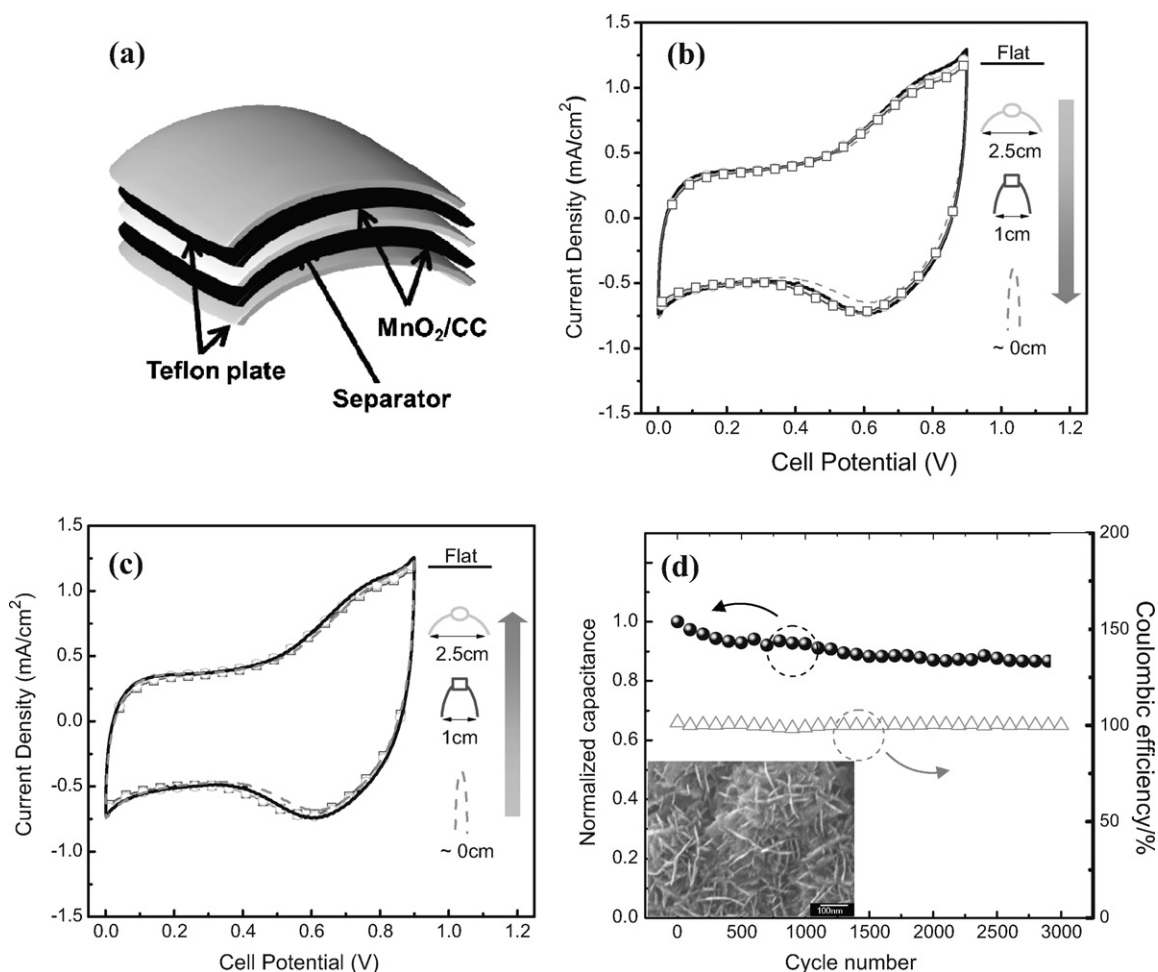


Fig. 6. (a) Schematic of the flexible supercapacitor made of MnO_2/CC , using a conventional two-electrode system. (b) MnO_2 capacitor bended with diameters of curvatures from 2.5 cm to 0 cm. (c) MnO_2 capacitor returned the diameters from 0 cm to 2.5 cm at a scan rate of 10 mV s^{-1} . (d) Cycle life of bent MnO_2 capacitor; inset, FESEM micrograph of MnO_2/CC hybrid electrode after cycle life test.

3.3. Capacitive properties

Electrochemical characteristics of the MnO_2 nanosheet/CC electrodes prepared for different deposition periods were evaluated by using cyclic voltammetry (CV) and galvanostatic charge/discharge methods. Fig. 5a presents the CV curves for various electrodes, measured in $0.1 \text{ M Na}_2\text{SO}_4$ electrolyte at 25°C with a potential scan rate of 25 mV s^{-1} . As can be observed, all CV curves are essentially close to rectangular shape and display symmetrical current-potential characteristics of a capacitor, except at potentials near the two extremes of the potential window. The mirror-image like characteristics of the anodic and cathodic regimes suggest an ideal pseudocapacitive behavior of the MnO_2 nanosheet/CC electrodes, whereas the areas enclosed under the CV curves correspond to energy storage capability of the MnO_2 nanosheet/CC electrodes. More significantly, the voltammetric current response, and consequently the capacitance of the coating, increased substantially with increase in deposition time from 500 s up to 2000 s. However, degradation in the voltammetric current accompanying with a distorted CV curve was observed for the thicker MnO_2 coating at deposition time of 2500 s, presumably due to the poor utilization of electroactive species and reduced active surface area of MnO_2 at this thickness [38].

To further examine the capacitive properties of hybrid MnO_2 nanosheet/CC electrodes, Fig. 5b compares the charge-discharge plots of the coatings corresponding to different deposition peri-

ods at a fixed current density of 0.13 mA cm^{-2} , within the potential window of 0–0.8 V. The anodic charging segments were generally symmetric to their corresponding cathodic discharging counterparts for all the samples, indicating a high reversibility of a typical capacitive material, consistent with CV observations reported earlier. The area-normalized capacitance (C_a) of an electrode in a given electrolyte solution can be calculated using an equation as follows:

$$C_a = \frac{i \Delta t}{A \Delta V}$$

where i is the discharge current for the applied time duration Δt , ΔV is the potential window, and A is the electrode area. Fig. 5c presents the area-normalized capacitance of MnO_2 nanosheet/CC electrodes as a function of deposition times. Note that the mass of MnO_2 deposited on the CC substrates was directly proportional to the deposition time. For deposition time of up to 2000 s, the capacitance showed linear increase with deposited mass with an optimal capacitance of 230 mF cm^{-2} . The capacitance, however, decreased for deposition times exceeding 2000 s, which can be attributed to aggregation of the MnO_2 nanosheets. Thus, it appears that deposition time of 2000 s is optimum for achieving maximum capacitance and acceptable characteristics for application as supercapacitors. In order to compare the present results and those reported in the literature, capacitance per mass of the coating (C_m) was also calculated. The optimum specific capacitance achieved in this study is as

high as 425 F g^{-1} , which is higher than many of the data reported in the literature [15,20], suggesting that the simple electrochemical process proposed in this study for MnO_2 deposition is promising for fabrication of MnO_2 nanosheet/CC composite electrodes with superior pseudocapacitive performance. Moreover, only 37% of loss in specific capacitance upon increasing the scan rate, as shown in Fig. 5d, can be ascribed to the hierarchical nanocomposite electrodes. The high gravimetric capacitance and enhanced stability can be attributed to the direct-growth approach employed to fabricate the MnO_2 nanosheet/CC composite electrodes. This approach can offer less resistive pathways for efficient electron transport along with improved utilization of MnO_2 . Similar direct-growth approach has been employed to RuO_2 and PANI, the other two popularly studied materials in the field of supercapacitors; superb gravimetric capacitance values as high as 1380 F g^{-1} and 1079 F g^{-1} , respectively, were reported in those cases [2,6].

In order to test the mechanical bendability of these electrodes and its effect on the capacitance, the schematic diagram of the flexible supercapacitor made of MnO_2 nanosheet/CC with cellulose film as separator by sandwiching the MnO_2 electrodes and 0.1 M Na_2SO_4 as the electrolyte is shown in Fig. 6a using a two-electrode system. Comparison of MnO_2 capacitors bended with diameters of curvature from 2.5 cm to 0 cm (Fig. 6b) and MnO_2 capacitors returned the diameters from 0 cm to 2.5 cm (Fig. 6c) at a scan rate of 10 mV s^{-1} showed similar capacitive behavior with capacitance loss only of 0.05%, demonstrating a highly bendable MnO_2 nanosheet/CC electrode with excellent mechanical stability. The reason for such superior mechanical performance can be ascribed to the efficient release of bending stress by nano-sized MnO_2 through inter-cluster gap adjustment. Furthermore, the specific discharge capacitance of bent MnO_2 capacitors as a function of the number of galvanostatic charge/discharge cycles is presented in Fig. 6d, which shows that the specific discharge capacitance decreased by about 6% during the first 1000 cycles, presumably related to the equilibration of electrode potential. Once the system is stabilized, the discharge capacitance displayed a constant magnitude through the next 2000 cycles. On the other hand, the coulombic efficiency, which is the ratio of charge capacitance to discharge capacitance, remained constant at 98.5% through the entire 3000 cycles. After galvanostatic charge/discharge cycles, the morphology of MnO_2 on CC, as shown in inset of Fig. 6d, still preserved without obvious damages as compared with pristine sample. Thus, excellent cycle life-time for MnO_2 capacitors under bending is demonstrated in this study, promising towards their potential application as flexible supercapacitor.

4. Conclusions

Hierarchically porous Birnessite-type MnO_2 nanosheets on CC substrates have been synthesized by anodic electrodeposition method for application as flexible electrode. The layered MnO_2 nanosheet/CC hybrid electrode with strong adhesion is shown to consist of petal-shaped MnO_2 in smaller units that form the cluster, with the sheet thickness of few nm and $\sim 100 \text{ nm}$ in width. The amenability of these clusters consequently benefits the release of bending stress. The optimal specific capacitance of the MnO_2 nanosheet/CC hybrid electrode is 425 F g^{-1} , which is higher than most of the literature reports. Moreover, such a high capacitance performance can be maintained under highly bended configuration, and excellent cycle life-time of over 3000 cycles of galvanostatic charge/discharge process under the bending test

is also demonstrated. The present results demonstrate that the petal-shape MnO_2 /CC is a promising active material for large-scale, flexible and electrochemically stable supercapacitor.

Acknowledgements

This research was financially supported by the Ministry of Education, Asian Office of Aerospace Research and Development under AFOSR, National Science Council, National Taiwan University, and Academia Sinica, Taiwan.

References

- [1] K.T. Nam, D.W. Kim, P.J. Yoo, C.Y. Chiang, N. Meethong, P.T. Hammond, Y.M. Chiang, A.M. Belcher, *Science* 312 (2006) 885.
- [2] Y.Y. Horng, Y.C. Lu, Y.K. Hsu, C.C. Chen, L.C. Chen, K.H. Chen, *J. Power Sources* 195 (2010) 4418.
- [3] V.L. Pushparaj, M.M. Shaijumon, A. Kumar, S. Murugesan, L.J. Ci, R. Vajtai, R.L. Linhardt, O. Nalamasu, P.M. Ajayan, *Proc. Natl. Acad. Sci. U.S.A.* 104 (2007) 13574.
- [4] P. Simon, Y. Gogotsi, *Nat. Mater.* 7 (2008) 845.
- [5] J.R. Miller, P. Simon, *Science* 321 (2008) 651.
- [6] W.C. Fang, O. Chyan, C.L. Sun, C.T. Wu, C.P. Chen, K.H. Chen, L.C. Chen, J.H. Huang, *Electrochem. Commun.* 9 (2007) 239.
- [7] R.F. Zhou, C.Z. Meng, F. Zhu, Q.Q. Li, C.H. Liu, S.S. Fan, K.L. Jiang, *Nanotechnology* 21 (2010) 345701.
- [8] B.E. Conway, *Electrochemical Supercapacitors, Scientific Fundamentals, Technological Applications*, 1st ed., Kluwer Academic Plenum Publisher, NY, 1999.
- [9] M. Toupin, T. Brousse, D. Belanger, *Chem. Mater.* 16 (2004) 3184.
- [10] S.L. Kuo, N.L. Wu, *J. Electrochem. Soc.* 153 (2006) A1317.
- [11] L. Athouel, F. Moser, R. Dugas, O. Crosnier, D. Belanger, T. Brousse, *J. Phys. Chem. C* 112 (2008) 7270.
- [12] Y.K. Hsu, Y.C. Chen, Y.G. Lin, L.C. Chen, K.H. Chen, *Chem. Commun.* 47 (2011) 1253.
- [13] C.C. Hu, K.H. Chang, M.C. Lin, Y.T. Wu, *Nano Lett.* 6 (2006) 2690.
- [14] A.E. Fischer, K.A. Pettigrew, D.R. Rolison, R.M. Stroud, J.W. Long, *Nano Lett.* 7 (2007) 281.
- [15] H. Zhang, G.P. Cao, Z.Y. Wang, Y.S. Yang, Z.J. Shi, Z.N. Gu, *Nano Lett.* 8 (2008) 26640.
- [16] Y.G. Hwang, H.Q. Li, Y.Y. Xia, *Adv. Mater.* 18 (2006) 2619.
- [17] G.Z. Hughes, M.S. Chen, P. Shaffer, D.J. Fray, A.H. Windle, *Chem. Mater.* 14 (2002) 1610.
- [18] T. Brousse, P. Taberna, O. Crosnier, R. Dugas, P. Guillemet, Y. Scudeller, Y. Zhou, F. Favier, D. Belanger, P. Simon, *J. Power Source* 173 (2007) 633.
- [19] V. Khomenko, E. Raymundo-Pinero, F. Beguin, *J. Power Source* 153 (2006) 183.
- [20] M.Q. Wu, L.P. Zhang, J.H. Gao, Y. Zhou, S.R. Zhang, A. Chen, *J. Electrochem. Soc.* 155 (2008) A355.
- [21] S.B. Ma, K.Y. Ahn, E.S. Lee, K.H. Oh, K.B. Kim, *Carbon* 45 (2007) 375.
- [22] J.T. Sampathar, J. Dou, G.G. Joo, E. Widjaja, L.Q.H. Eunice, *Nanotechnology* 18 (2007) 025601.
- [23] W.F. Wei, X.W. Cui, W.X. Chen, D.G. Ivey, *J. Phys. Chem. C* 112 (2008) 15075.
- [24] S.L. Chou, F.Y. Cheng, J. Chen, *J. Power Source* 162 (2006) 727.
- [25] C.C. Hu, K.H. Chang, Y.T. Wu, C.Y. Hung, C.C. Lin, Y.T. Tsai, *Electrochem. Commun.* 10 (2008) 1792.
- [26] C.C. Hu, C.Y. Hung, K.H. Chang, Y.L. Yang, *J. Power Sources* 196 (2011) 847.
- [27] J. Yan, Z. Fan, T. Wei, J. Cheng, B. Shao, K. Wang, L. Song, M. Zhang, *J. Power Sources* 194 (2009) 1202.
- [28] Y. Ma, J. Luo, S.L. Suib, *Chem. Mater.* 11 (1999) 1972.
- [29] J.K. Chang, S.H. Hsu, W.T. Tsai, I.W. Sun, *J. Power Source* 177 (2008) 676.
- [30] T. Shinomiya, V. Gupta, N. Miura, *Electrochim. Acta* 51 (2006) 4412.
- [31] H. Zheng, F. Tang, Y. Jia, L. Wang, Y. Chen, M. Lim, L. Zhang, G. Lu, *Carbon* 47 (2009) 1534.
- [32] S.W. Lee, B.S. Kim, S. Chen, S.H. Yang, P.T. Hammond, *J. Am. Chem. Soc.* 131 (2009) 671.
- [33] C.H. Wang, H.Y. Du, Y.T. Tsai, C.P. Chen, C.J. Huang, L.C. Chen, K.H. Chen, H.C. Shih, *J. Power Source* 171 (2007) 55.
- [34] Y.K. Hsu, J.L. Yang, Y.K. Lin, S.Y. Chen, L.C. Chen, K.H. Chen, *Diamond Relat. Mater.* 18 (2009) 557.
- [35] Y.C. Hsieh, K.T. Lee, Y.P. Lin, N.L. Wu, S.W. Donne, *J. Power Source* 177 (2008) 660.
- [36] C. Julien, M. Massot, R. Baddour-Hadjean, S. Franger, S. Bach, J.P. Pereira-Ramos, *Solid State Ionics* 159 (2008) 345.
- [37] M. Nakayama, S. Konoshi, H. Tagashira, K. Ogura, *Langmuir* 21 (2005) 354.
- [38] Y.T. Wu, C.C. Hu, *J. Electrochem. Soc.* 151 (2004) A2060.